On the dynamics of non-local fractional viscoelastic beams under stochastic agencies

Gioacchino Alotta[a,*], Mario Di Paola[b], Giuseppe Failla[c], Francesco Paolo Pinnola[d]

[a]*Engineering and Architecture Faculty, University of Enna "Kore", Viale delle Olimpiadi, 94100 Enna, Italy.*
[b]*Department of Civil, Environment, Aerospace, Materials Engineering (DICAM), University of Palermo, Palermo, Italy*
[c]*Departiment of Civil, Energy, Environment, Materials Engineering (DICEAM), University of Reggio Calabria, Via Graziella, Localitá Feo di Vito, 89124 Reggio Calabria, Italy.*
[d]*Department of Innovation Engineering, University of Salento, Lecce, Italy.*

Abstract

Non-local viscoelasticity is a subject of great interest in the context of non-local theories. In a recent study, the authors have proposed a non-local fractional beam model where non-local effects are represented as viscoelastic long-range volume forces and moments, exchanged by non-adjacent beam segments depending on their relative motion, while local effects are modelled by elastic classical stress resultants. Long-range interactions have been given a fractional constitutive law, involving the Caputo's fractional derivative. This paper introduces a comprehensive numerical approach to calculate the stochastic response of the non-local fractional beam model under Gaussian white noise. The approach combines a finite-element discretization with a fractional-order state-variable expansion and a complex modal transformation to decouple the discretized equations of motion. While closed-form expressions are derived for the finite-element matrices associated with elastic and fractional terms, fractional calculus is used to solve the decoupled fractional equations of motion, in both time and frequency domain. Remarkably, closed-form expressions are obtained for the power spectral density, cross power spectral density, variance and covariance of the beam response along the whole axis. Time-domain solutions are obtained by time-step numerical integration methods involving analytical expressions of impulse response functions. Numerical examples show versatility of the non-local fractional model as well as computational advantages of the proposed solution procedure.

Keywords: Non local Timoshenko beam, Fractional viscoelasticity, White noise, State variable expansion

1. Introduction

There exists a great variety of non-local beam models in recent literature [1–13], used in a wide range of engineering problems. Certainly a well-established application field is micro- and nano-engineering [12–25], where non-local beam models with various degree of complexity have been proposed as alternative to computationally expensive and sometimes even prohibitive molecular simulations [26], in order to capture size effects which cannot be addressed by a classical local continuum approach [12–25].
Existing non-local beam models typically involve non-local stiffness terms [1–13, 17, 18, 21–25], but also non-local damping terms have been considered in recent studies [28–37]. Typical examples of non-local damping at a macro-scale are those associated with external damping patches applied on beams, surface treatments, long adhesive joints or fibres in composites, which may produce a long-range damped coupling between non-adjacent points of the composite [28–33]. On the other hand, non-local damping models may be useful for capturing damping effects at micro-and nano-scale [34–37], which proved to be relevant in image acquisition via high-speed atomic force microscopes [38] and frequency measurements of vibrating nano-sensors [39]; damping effects in nanostructures have also been observed as a result of humidity and thermal effects [40], external magnetic forces [41], or in tensile test on graphene

*Corresponding author at: Engineering and Architecture Faculty, University of Enna "Kore", Viale delle Olimpiadi, 94100 Enna, Italy.
Email addresses: gioacchino.alotta@unikore.it (Gioacchino Alotta), mario.dipaola@unipa.it (Mario Di Paola), giuseppe.failla@unirc.it (Giuseppe Failla), francesco.pinnola@unisalento.it (Francesco Paolo Pinnola)

oxide nanoplates [42].
In the last years, the authors have proposed a non-local beam model, where non-local effects are represented as long-range volume forces and moments mutually exchanged by non-adjacent beam segments, while local effects are modelled by the classical local stress resultants [43–46]. The long-range forces/moments are built as depending on the volumes of the interacting beam segments, and their relative motion measured by the pure deformation modes of the beam, through distance-decaying attenuation functions. Elastic or viscoelastic long-range interactions have been considered, the latter with classical Kelvin-Voigt constitutive law [46]. In a more recent paper [47], long-range volume forces and moments have been modelled by the authors with a fractional constitutive law using, in particular, the Caputo's fractional derivative [48]. For their capability of representing a wide range of viscoelastic behaviours, fractional operators seem indeed particularly appropriate to build theoretical non-local models that may handle a large variety of non-local viscoelastic effects, ranging from the nano- to the macro-scale. In ref. [47], however, numerical solutions have been presented only for the creep response and neglecting inertial effects. Yet, in order to calculate the response of the non-local beam model in more general cases, an effective numerical procedure is certainly required. Ideally, it should avoid time-consuming numerical integrations which are typically involved when solving fractional multi-degree-of-freedom equations of motion and, at the same time, it should be easy to implement also for engineers who are not necessarily familiar with fractional calculus. In this context, solution procedures for computing the stochastic response are of particular interest, in view of possible applications for modelling non-local viscoelastic response of nano-devices as sensors or resonators.

The purpose of this paper is to introduce a comprehensive numerical approach to calculate the stochastic response of the non-local fractional Timoshenko beam model in ref. [47], under a Gaussian white noise input. The approach relies on a finite-element (FE) discretization in conjunction with a fractional-order state-variable expansion and a complex modal transformation to decouple the discretized fractional equations of motion. Closed-form expressions are derived for FE matrices associated with elastic and fractional terms. Pertinent analytical tools of fractional calculus are used to solve the decoupled equations of motion, providing an efficient solution in time and frequency domain. Time-domain solutions are obtained by standard numerical integration procedures involving closed-form impulse response functions. Frequency-domain solutions are used to build novel exact analytical expressions for the power spectral density (PSD), cross power spectral density (CPSD), variance, and covariance of the beam response along the whole axis. The numerical approach proposed in this paper mirrors the numerical approach used by the authors in ref. [49] for studying the axial vibrations of a non-local fractional bar. A main novelty with respect to ref. [49], however, is the exact closed-form expression here obtained for the PSD/CPSD and variance/covariance of the beam response, which may represent a useful benchmark for any alternative numerical approach. The paper is organized as follows. Section 2 recalls the key concepts of the non-local fractional beam model and the corresponding FE equations of motion. The proposed numerical approach for computing the stochastic response of the non-local beam model is presented in Section 3. Finally, numerical applications are discussed in Section 4.

2. Non-local fractional beam model

Here the non-local fractional beam model is briefly recalled, along with the pertinent FE formulation. More details may be found in ref. [45] of the authors.

2.1. Equation of motion

Consider the uniform beam in Fig. 1, referred to a reference system where x and y are principal axes for the cross section with area A, z is the centroidal axis. Under the assumptions of small displacements, the kinematics of the Timoshenko beam is described by the following relations:

$$\chi(z,t) = -\frac{\partial \varphi(z,t)}{\partial z}; \quad \gamma(z,t) = \frac{\partial v(z,t)}{\partial z} - \varphi(z,t) \tag{1}$$

where v is the deflection in y direction, φ is the rotation of the cross section about the x axis, χ is the curvature and γ is the shear strain. The local resultants are written as

$$T_y^{(l)}(z,t) = \int_A \tau_{xy}(x,y,z,t)dA = G^* K_s A \gamma(z,t); \quad M_x^{(l)}(z,t) = \int_A \sigma_z(x,y,z,t) y dA = E^* I_x \chi(z,t) \tag{2}$$

where $T_y^{(l)}$ is the local shear resultant in y direction, τ_{xy} is the shear stress, K_s is the shear factor, $M_x^{(l)}$ is th local bending resultant, σ_z is the local stress in the z direction, I_x is the moment of inertia about the x axis, $E^* = \beta_1 E$, $G^* = \beta_1 G$ where E is the Young's modulus, G is the shear modulus, β_1 is a dimensionless parameter with values in the range $0 \div 1$, that reduces the amount of local effects [44]. Regarding non-local effects, the key assumption is that

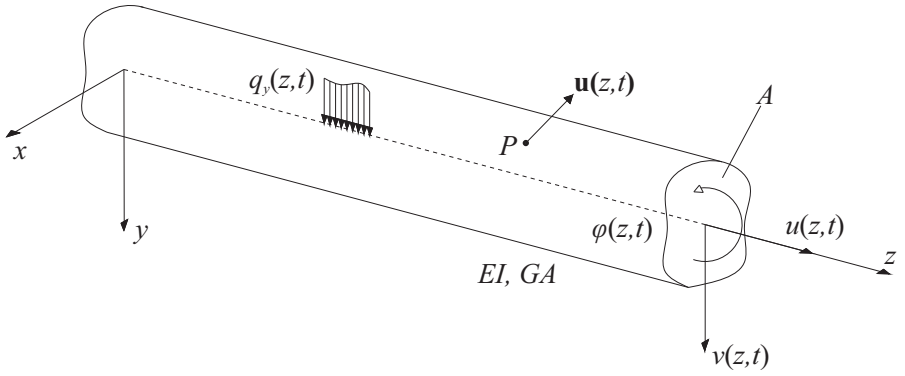

Figure 1: Non local beam.

non-adjacent beam segments mutually exert long-rangeforces and moments due to relative motion. More specifically, consider two non-adjacent beam segment of volume $\Delta V(z_i)$ and $\Delta V(\zeta_k)$ located at the positions $z = z_i$ and $z = \zeta_k$ on the beam longitudinal axis, respectively; it is assumed that they mutually exert long-range forces and moments as a consequence of their relative motion measured by the pure deformation modes of the beam [50]. The long-range forces/moments are supposed to be self-equilibrated according to the Newton's third law. They are taken as linearly depending on the product of the two interacting volumes and an attenuation function governing the decay of non-local effects with the relative distance. In the model, both purely elastic and fractional viscoelastic forces, modeled by Caputo's fractional derivative, are considered. A mechanical description of the long range interactions is provided in Fig. 2.

In Fig. 2.1 the pure deformations θ and ψ are defined as follows:

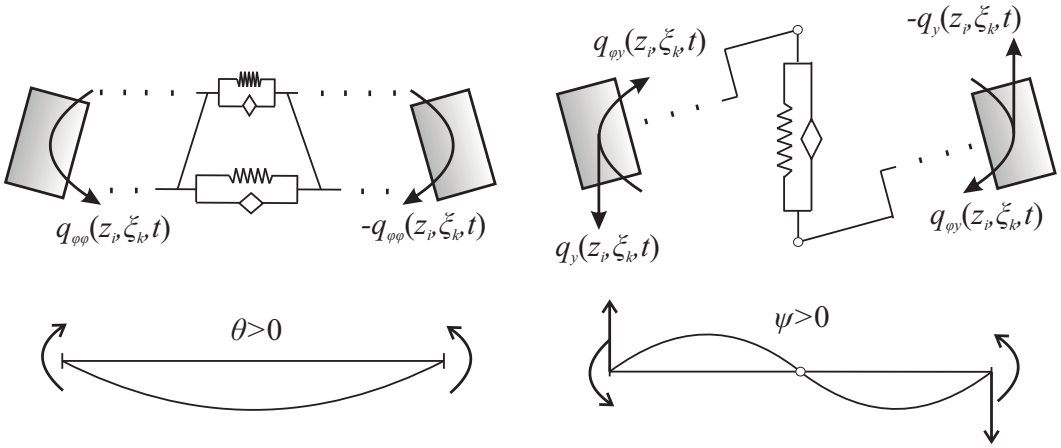

Figure 2: Pure mode of deformation.

$$\theta(z_i,\zeta_k,t) = \varphi(\zeta_k,t) - \varphi(z_i,t); \qquad \psi(z_i,\zeta_k,t) = \frac{v(\zeta_k,t) - v(z_i,t)}{\zeta_k - z_i} + \varphi(\zeta_k,t) + \varphi(z_i,t) \tag{3}$$

The bending moments exchanged by the two volumes $\Delta V(z_i)$ and $\Delta V(\zeta_k)$, due to the pure bending rotation θ, are given as:

$$q_{\varphi\varphi}(z_i,\zeta_k,t) = r_{\varphi\varphi}(z_i,\zeta_k,t) + d_{\varphi\varphi}(z_i,\zeta_k,t) \tag{4a}$$

$$r_{\varphi\varphi}(z_i,\zeta_k,t) = g_{\varphi}(z_i,\zeta_k)\theta(z_i,\zeta_k,t)\Delta V(z_i)\Delta V(\zeta_k) \tag{4b}$$

$$d_{\varphi\varphi}(z_i,\zeta_k,t) = \tilde{g}_{\varphi}(z_i,\zeta_k)\left(\left(D^{\alpha}_{0^+}\theta\right)(z_i,\zeta_k,t)\right)\Delta V(z_i)\Delta V(\zeta_k) \tag{4c}$$

The forces mutually exerted by the two volumes $\Delta V(z_i)$ and $\Delta V(\zeta_k)$, due to the pure shear deformation ψ, are given as:

$$q_{y}(z_i,\zeta_k,t) = r_{y}(z_i,\zeta_k,t) + d_{y}(z_i,\zeta_k,t) \tag{5a}$$

$$r_{y}(z_i,\zeta_k,t) = \frac{1}{|z_i-\zeta_k|}g_{y}(z_i,\zeta_k)\psi(z_i,\zeta_k,t)\Delta V(z_i)\Delta V(\zeta_k) \tag{5b}$$

$$d_{y}(z_i,\zeta_k,t) = \frac{1}{|z_i-\zeta_k|}\tilde{g}_{y}(z_i,\zeta_k)\left((D^{\alpha}_{0^+}\psi)(z_i,\zeta_k,t)\right)\Delta V(zx_i)\Delta V(\zeta_k) \tag{5c}$$

whereas the moments are

$$q_{\varphi y}(z_i,\zeta_k,t) = r_{\varphi y}(z_i,\zeta_k,t) + d_{\varphi y}(z_i,\zeta_k,t) \tag{6a}$$

$$r_{\varphi y}(z_i,\zeta_k,t) = g_{y}(z_i,\zeta_k)\psi(z_i,\zeta_k,t)\Delta V(z_i)\Delta V(\zeta_k) \tag{6b}$$

$$d_{\varphi y}(z_i,\zeta_k,t) = \tilde{g}_{y}(z_i,\zeta_k)\left((D^{\alpha}_{0^+}\psi)(z_i,\zeta_k,t)\right)\Delta V(z_i)\Delta V(\zeta_k) \tag{6c}$$

In Eqs.(4)-(6), symbols $r_{\varphi\varphi}$ and r_y denote the elastic long-range interactions, while $d_{\varphi\varphi}$ and d_y indicate the fractional ones. Specifically, symbol $D^{\alpha}_{0^+}$ denotes the Caputo's fractional derivative, defined as [40]:

$$\left(D^{\alpha}_{0^+}u\right)(t) = \frac{1}{\Gamma(1-\alpha)}\int_0^t (t-\tau)^{-\alpha}\dot{u}(\tau)d\tau \tag{7}$$

where $0 \leq \alpha \leq 1$ and C_α are material parameters, while $\Gamma(\cdot)$ is the Euler gamma function. Further, symbols g_φ and $\tilde{g}_\varphi$ in Eqs.(6) denote the attenuation functions of the pure-bending elastic and fractional long-range interactions respectively, while g_y and $\tilde{g}_y$ in Eqs.(7)-(8) have the same meaning for the pure-shear long-range interactions. Typically, they are chosen as Gaussian, exponential or power law functions [45, 51]. The model allows different attenuation functions for pure-bending and pure-shear long-range effects, as well as elastic and fractional ones. Next, let us divide the beam in N segments of length Δz and consider the bar segment of $\Delta V(z_i) = A\Delta z$ at the location $z_i = i\Delta z$, with $i = 0,1,...,N$; the equations of motion of this bar segment are

$$T^{(l)}(z_i+\Delta z,t) - T^{(l)}(z_i,t) + R_y(z_i,t) + F_y(z_i,t)\Delta z - \rho(x_i)A\ddot{v}(z_i,t)\Delta z = 0 \tag{8a}$$

$$M^{(l)}(z_i+\Delta z,t) - M^{(l)}(z_i,t) + R_\varphi(z_i,t)\Delta z - \rho I_x\ddot{\varphi}(z_i,t)\Delta z = 0 \tag{8b}$$

where $q_y(z_i,t)$ is the external force per unit-length, $m(x) = \rho(x)A$ being $\rho(x)$ the mass per unit volume and R_y and R_φ are the resultants of non-local forces and moments on the beam segment written as

$$R_y(z_i,t) = \sum_{k=0,k\neq i}^{N-1} q_y(z_i,\zeta_k,t); \qquad R_\varphi(z_i,t) = \sum_{k=0,k\neq i}^{N-1} q_{\varphi\varphi}(z_i,\zeta_k,t) + q_{\varphi y}(z_i,\zeta_k,t) \tag{9}$$

Considering Eqs. (9), dividing Eqs. (8) by Δz and taking the limit for $\Delta z \to 0$, the continuous counterparts of Eqs. (8) are obtained:

$$\chi GA\left[\frac{\partial^2 u(z,t)}{\partial z^2} + \frac{\partial\varphi(z,t)}{\partial z}\right] + q_y(z,t) + \int_0^L \frac{2}{\zeta - z}\left\{g_y(z,\zeta)\psi(z,\zeta,t) + \tilde{g}_y(z,\zeta)\left((D^{\alpha}_{0^+}\psi)(z,\zeta,t)\right)\right\}d\zeta = \rho A\ddot{v}(z,t) \tag{10a}$$

$$EI_x\frac{\partial^2\varphi(z,t)}{\partial z^2}+\chi GA\left[\frac{\partial u(z,t)}{\partial z}+\varphi(z,t)\right]+A^2\int_0^L\left\{g_\varphi(z,\zeta)\theta(z,\zeta,t)+\tilde{g}_\varphi(z,\zeta)D_{0^+}^{\alpha}\left[\theta(z,\zeta,t)\right]\right\}dz$$
$$+A^2\int_0^L\left\{g_y(z,\zeta)\psi(z,\zeta,t)+\tilde{g}_y(z,\zeta)\left((D_{0^+}^{\alpha}\psi)(z,\zeta,t)\right)\right\}dz=\rho I_x\ddot{\varphi}(z,t) \quad (10b)$$

The boundary conditions (BCs) hold the same form of classical local theory as it may readily be seen that, in the equilibrium equations at the beam ends, the long-range forces and moments are infinitesimal of higher order with respect to the local stress resultants [43]. Therefore, the BCs are:

$$\chi GA\left[\frac{\partial u(z,t)}{\partial z}+\varphi(z,t)\right]_{z=z_i}=\mp T_i(t) \quad or \quad v(z_i,t)=v_i(t) \quad (11a)$$

$$EI_x\left.\frac{\partial\varphi(z,t)}{\partial z}\right|_{z=z_i}=\mp M_i(t) \quad or \quad \varphi(z_i,t)=\varphi_i(t) \quad (11b)$$

2.2. Finite-element formulation

The non-local fractional beam model is suitable for implementation in FE method. For this purpose, let us divide the total length ot the beam in n FEs of the same length l, such that $nl=L$, being L the total length of the beam. The points shared by adjacent FEs are the nodes; the generic $i-th$ element has two nodes at $z=\hat{z}_i=(i-1)l$ and $z=\hat{z}_{i+1}=il$. The displacement field within the element is represented by means of standard linear shape functions as follows:

$$\boldsymbol{u}_i(z,t)=\boldsymbol{N}_i(z)\boldsymbol{d}_i(t); \qquad \boldsymbol{d}_i^{\mathrm{T}}(t)=\left[v_{(i)1}(t)\ \varphi_{(i)1}(t)\ v_{(i)2}(t)\ \varphi_{(i)2}(t)\right] \quad (12)$$

where $i=1,2,...,n,$, $v_{(i)1,2}(t)$ and $\varphi_{(i)1,2}(t)$, are deflections and rotations of the two nodes of the $i-th$ element and $\boldsymbol{N}_i(x)$ is the shape functions matrix of the $i-th$ element, that is

$$\boldsymbol{N}_i^{\mathrm{T}}(z)=\begin{bmatrix}\frac{(l-\delta_i)\left(l^2(1+12\Omega)+(l-2\delta_i)\delta_i\right)}{l^3(1+12\Omega)} & \frac{6(l-\delta_i)\delta_i}{l^3(1+12\Omega)}\\ -\frac{(l-\delta_i)(l+6l\Omega-\delta_i)\delta_i}{l^2(1+12\Omega)} & \frac{(l+12l\Omega-3\delta_i)(l-\delta_i)}{l^2(1+12\Omega)}\\ \frac{\delta_i(12l^2\Omega+3l\delta_i-2\delta_i^2)}{l^3(1+12\Omega)} & \frac{6(\delta_i-l)\delta_i}{l^3(1+12\Omega)}\\ \frac{(l-\delta_i)(6l\Omega+\delta_i)\delta_i}{l^2(1+12\Omega)} & \frac{(2l(1-6\Omega)+3\delta_i)\delta_i}{l^2(1+12\Omega)}\end{bmatrix} \quad (13)$$

where $\delta_i=z-\hat{z}_i$. Next, being $\boldsymbol{d}^{\mathrm{T}}(t)=[u_1(t)\ \ \varphi_1(t)\ \ u_2(t)\ \ \varphi_2(t)\ldots\varphi_{n+1}(t)]$ the vector collecting the displacements of all nodes, the nodal displacements of the $i-th$ element are written as $\boldsymbol{d}_i(t)=\boldsymbol{C}_i\boldsymbol{d}(t)$ where C_i is the connectivity matrix of the $i-th$ element. Following a standard Galerkin approach, the dynamic equilibrium equation of the discretized beam is

$$\boldsymbol{M}\ddot{\boldsymbol{d}}(t)+\boldsymbol{C}^{(nl)}\left((D^{\alpha}\boldsymbol{d})(t)\right)+\boldsymbol{K}\boldsymbol{d}(t)=\boldsymbol{F}(t), \quad (14)$$

being $\boldsymbol{M}$ the consistent mass matrix, $\boldsymbol{C}^{(nl)}$ the matrix of fractional long range interactions, $\boldsymbol{K}$ the stiffness matrix and $\boldsymbol{F}(t)$ the vector of nodal forces. The stiffness matrix is obtained as

$$\boldsymbol{K}=\boldsymbol{K}^{(l)}+\boldsymbol{K}^{(nl)}=\sum_{i=1}^{n}\boldsymbol{K}_i^{(l)}+\sum_{i=1}^{n}\boldsymbol{K}_i^{(nl)}, \quad (15)$$

where $\boldsymbol{K}^{(l)}$ and $\boldsymbol{K}^{(nl)}$ are the local and non-local contributions, respectively. The local stiffness matrix of the $i-th$ element is

$$\boldsymbol{K}_i^{(l)}=\int_{\hat{z}_i}^{\hat{z}_{i+1}}\left[\boldsymbol{B}_i(z)\boldsymbol{C}_i\right]^{\mathrm{T}}\boldsymbol{D}\boldsymbol{B}_i(z)\boldsymbol{C}_i dz, \quad (16)$$

where $\boldsymbol{D}=\mathrm{D}iag\left[EI_x\ \ \chi GA\right]$ and $\boldsymbol{B}_i(z)$ is the vector collecting the spatial derivative of the shape functions, while $\boldsymbol{K}_i^{(nl)}$ is

$$\boldsymbol{K}_i^{(nl)}=\boldsymbol{K}_i^{(nl,\theta)}+\boldsymbol{K}_i^{(nl,\psi)}=\sum_{j=1}^{n}\boldsymbol{K}_{ij}^{(nl,\theta)}+\sum_{j=1}^{n}\boldsymbol{K}_{ij}^{(nl,\psi)} \quad (17)$$

with

$$\boldsymbol{K}_{ij}^{(nl,\theta)} = \frac{A^2}{2}\int_{\hat{z}_i}^{\hat{z}_{i+1}}\int_{\hat{z}_j}^{\hat{z}_{j+1}} \left[\boldsymbol{N}_j^{(\varphi)}(\zeta)\boldsymbol{C}_j - \boldsymbol{N}_i^{(\varphi)}(z)\boldsymbol{C}_i\right]^{\mathrm{T}} g_\varphi(z,\zeta)\left[\boldsymbol{N}_j^{(\varphi)}(\zeta)\boldsymbol{C}_j - \boldsymbol{N}_i^{(\varphi)}(z)\boldsymbol{C}_i\right] dz d\zeta \tag{18a}$$

$$\boldsymbol{K}_{ij}^{(nl,\psi)} = \frac{A^2}{2}\int_{\hat{z}_i}^{\hat{z}_{i+1}}\int_{\hat{z}_j}^{\hat{z}_{j+1}} \left[2\left(\boldsymbol{N}_j^{(v)}(\zeta)\boldsymbol{C}_j - \boldsymbol{N}_i^{(v)}(z)\boldsymbol{C}_i\right)/(\zeta - z) + \boldsymbol{N}_j^{(\varphi)}(\zeta)\boldsymbol{C}_j + \boldsymbol{N}_i^{(\varphi)}(z)\boldsymbol{C}_i\right]^{\mathrm{T}}$$
$$g_y(z,\zeta)\left[2\left(\boldsymbol{N}_j^{(v)}(\zeta)\boldsymbol{C}_j - \boldsymbol{N}_i^{(v)}(z)\boldsymbol{C}_i\right)/(\zeta - z) + \boldsymbol{N}_j^{(\varphi)}(\zeta)\boldsymbol{C}_j + \boldsymbol{N}_i^{(\varphi)}(z)\boldsymbol{C}_i\right] dz d\zeta \tag{18b}$$

It is to emphasized that the matrix $\boldsymbol{C}^{(nl)}$ has the same mathematical form of the non-local stiffness matrix $\boldsymbol{K}^{(nl)}$, the only difference being that $\boldsymbol{C}^{(nl)}$ involves $\tilde{g}_i(z,\zeta)$ instead of $g_i(z,\zeta)$. Finally, the vector $\boldsymbol{F}(t)$ is given as:

$$\boldsymbol{F}(t) = \sum_{i=1}^{n}\int_{V_i}[\boldsymbol{N}_i(x)\boldsymbol{C}_i]^{\mathrm{T}}\bar{\boldsymbol{F}}(z,t)dV_i(x) + [\boldsymbol{N}_1(0)\boldsymbol{C}_i]^{\mathrm{T}}\bar{\boldsymbol{F}}_1(t) + [\boldsymbol{N}_{n+1}(L)\boldsymbol{C}_{n+1}]^{\mathrm{T}}\bar{\boldsymbol{F}}_{n+1}(t). \tag{19}$$

where $\bar{\boldsymbol{F}}(z,t) = [F_y(z,t)\ \ 0]$ and $\bar{\boldsymbol{F}}_i(t) = [T_i\ \ M_i]$, $i = 1, n+1$, being T_i and M_i external transverse forces and moments. It is important to remark that closed-form expressions for all terms in the non-local matrices $\boldsymbol{K}^{(nl)}$ and $\boldsymbol{C}^{(nl)}$ may be found in ref. [45] of the authors.

3. Stochastic response of non-local beam

In this section, the FE formulation of the fractional viscoelastic non-local beam introduced in the previous section is used to study the vibration of the dynamical system for the case in which the external load vector in Eq. (14) is composed by stochastic agencies. In particular, without loss of generality, suppose that each node of the beam is forced by a zero mean Gaussian white noise denoted by $W(t)$, therefore $\boldsymbol{F}(t) = \boldsymbol{p}W(t)$, being $\boldsymbol{p}$ an influence vector. Under this assumptions, the response vector is a set of stochastic response processes $\boldsymbol{d}^{\mathrm{T}}(t) = [V_1(t), \Phi_1(t), \ldots, V_{n+1}(t), \Phi_{n+1}(t)]$, where capital letters distinguish stochastic processes from deterministic ones. In this way the set of coupled differential equations in Eq. (14) becomes

$$\boldsymbol{M}\ddot{\boldsymbol{d}}(t) + \boldsymbol{C}^{(nl)}\left(D^{\alpha}\boldsymbol{d}\right)(t) + \boldsymbol{K}\boldsymbol{d}(t) = \boldsymbol{p}W(t), \tag{20}$$

where $W(t)$ is characterized by a constant PSD and by a Dirac delta function as Characteristic Function (CF). In particular,

$$S_W(\omega) = S_0, \qquad R_W(\tau) = 2\pi\delta(\tau) \tag{21}$$

being $\delta(\tau)$ the Dirac delta function, $S_W(\omega)$ the PSD and $R_W(\tau)$ the CF.

The system in Eq. (20) is linear, therefore, if the input processes are Gaussian also the output responses are Gaussian too. For this reason, each output process can be described at steady state by the PSD, and/or by its Fourier transform, that is the CF of the response. For the evaluation of the PSD the frequency analysis is particularly useful and also permits to find the stationary statistics of the response. In particular, with the aid of the Fourier transform, the Eq. (20) in frequency domains yields

$$\left[-\omega^2\boldsymbol{M} + (\mathrm{i}\omega)^{\alpha}\boldsymbol{C}^{(nl)} + \boldsymbol{K}\right]\boldsymbol{d}_{\mathscr{F}}(\omega,T) = \boldsymbol{p}W_{\mathscr{F}}(\omega,T) \tag{22}$$

where the $\mathrm{i} = \sqrt{-1}$ is the imaginary unit, $\boldsymbol{d}_{\mathscr{F}}(\omega,T)$ contains the truncated Fourier transform of the response processes, and $W_F(\omega,T)$ denotes the Fourier transform of the Gaussian white noises truncated at time T in the frequency domain ω. It is worth of notice that the power law $(\mathrm{i}\omega)^{\alpha}$, related to the fractional order terms, contains an effective stiffness (related to the real part of $(\mathrm{i}\omega)^{\alpha}$) and an effective damping (proportional to the imaginary part of $(\mathrm{i}\omega)^{\alpha}$). From Eq. (22) the response vector in the frequency domain $\boldsymbol{d}_{\mathscr{F}}(\omega,T)$ is

$$\boldsymbol{d}_{\mathscr{F}}(\omega,T) = \left[-\omega^2\boldsymbol{M} + (\mathrm{i}\omega)^{\alpha}\boldsymbol{C}^{(nl)} + \boldsymbol{K}\right]^{-1}\boldsymbol{p}W_{\mathscr{F}}(\omega,T) = \boldsymbol{H}(\omega)\boldsymbol{p}W_{\mathscr{F}}(\omega,T), \tag{23}$$

where $\boldsymbol{H}(\omega)$ is matrix that contains the transfer functions of the system.

In order to fully characterize the stationary response in terms of displacements $V_j(t)$ and rotation $\Phi_j(t)$ for $j = 1,2,\dots,n$ of the free degree-of-freedom, the evaluation of the PSD and all the cross PSD of each element of the vector $\boldsymbol{d}(t)$ is needed. In this regard, consider the PSD matrix defined as

$$\boldsymbol{S_d}(\omega) = \boldsymbol{H}^*(\omega)\boldsymbol{p}\lim_{T\to\infty}\frac{\mathrm{E}\left[W^*_{\mathscr{F}}(\omega,T)W_{\mathscr{F}}(\omega,T)\right]}{2\pi T}\boldsymbol{p}^{\mathrm{T}}\boldsymbol{H}^{\mathrm{T}}(\omega) = \boldsymbol{H}^*(\omega)\boldsymbol{p}S_0\boldsymbol{p}^{\mathrm{T}}\boldsymbol{H}^{\mathrm{T}}(\omega), \tag{24}$$

where $\mathrm{E}[\cdot]$ is the expectation value, and the apex * denotes the complex conjugate. Consequently, the matrix $\boldsymbol{S}_d(\omega)$ with dimension $2n\times 2n$ is defined as

$$\boldsymbol{S_d}(\omega) = \begin{bmatrix} S_{d,11}(\omega) & S_{d,12}(\omega) & \dots & S_{d,12n} \\ S_{d,21}(\omega) & S_{d,22}(\omega) & \dots & S_{d,22n} \\ \vdots & \vdots & \ddots & \vdots \\ S_{d2n1}(\omega) & S_{d,2n2}(\omega) & \dots & S_{d,2n2n} \end{bmatrix} = \begin{bmatrix} S_{V_1}(\omega) & S_{V_1\Phi_1}(\omega) & \dots & S_{V_1\Phi_n} \\ S_{\Phi_1V_1}(\omega) & S_{\Phi_1}(\omega) & \dots & S_{\Phi_1\Phi_n} \\ \vdots & \vdots & \ddots & \vdots \\ S_{\Phi_nV_1}(\omega) & S_{\Phi_n\Phi_1}(\omega) & \dots & S_{\Phi_n} \end{bmatrix} \tag{25}$$

and each term represents the PSD function of the output processes and their cross counterparts. In particular, the diagonal terms are the PSDs, whereas the other terms are the cross PSDs. The knowledge of each term of the matrix in Eq. (25) permits to evaluate also the correlation and cross-correlation function with the aid of the Wiener-Khinchin Theorem. That is,

$$\begin{aligned} S_{d,jk}(\omega) &= \frac{1}{2\pi}\int_{-\infty}^{\infty} R_{d,jk}(\tau)\exp(\mathrm{i}\omega\tau)d\tau, \\ R_{d,jk}(\tau) &= \int_{-\infty}^{\infty} S_{d,jk}(\omega)\exp(-\mathrm{i}\omega\tau)d\omega, \end{aligned} \tag{26}$$

where $R_{d,jk}(\tau)$ represents the cross correlation of the j-th and k-th response process. From the knowledge of the quantities in Eq. (26) the stationary variance and covariance can be found as

$$\sigma^2_{d,jk} = \int_{-\infty}^{\infty} S_{d,jk}(\omega)d\omega = R_{d,jk}(0). \tag{27}$$

Observe that the quantities in Eq. (25) provide a complete description at steady state of the Gaussian processes. Unfortunately, the PSD matrix, can be evaluated in analytical form only for a few number of degree of freedom. In fact, usually the matrix $\boldsymbol{H}(\omega)$ cannot be obtained by means of the matrix inversion in Eq. (23). Therefore, just a numerical evaluation of each terms of $\boldsymbol{S_d}(\omega)$ can be pursued by the discretization of the variable ω. For this reason in the next subsection the problem is solved with the introduction of a proper state variable expansion and a complex modal transformation in order to find the exact solution of each term in the PSD matrix. However, the numerical solution obtained with the aid of of Eq. (23) is used as a benchmark for the results obtained by the method in the next subsection.

3.1. Steady-state analysis

For the case at hand, the matrix inversion problem in Eq. (23) cannot be solved with the aid of a classical modal transformation, therefore other mathematical tools are needed. In this regards, consider the case in which the fractional order α is rational, under this assumptions it is possible to represent the generic fractional order as irreducible fractions of two integer values $\alpha = a/b$, where $a,b\in\mathbb{N}$. In this manner, the system in Eq. (22) can be rewritten as the following sequential linear algebraic equations:

$$\left[\sum_{j=1}^{2b}\boldsymbol{C}_j(\mathrm{i}\omega)^{j/b} + \boldsymbol{K}\right]\boldsymbol{d}_{\mathscr{F}}(\omega,T) = \boldsymbol{p}W_{\mathscr{F}}(\omega,T), \tag{28}$$

where the involved matrices in the summation are $\boldsymbol{C}_a = \boldsymbol{C}^{(nl)}$, $\boldsymbol{C}_{2b} = \boldsymbol{M}$ and $\boldsymbol{C}_j = \boldsymbol{0}$, $\forall j : j\in(1,a]$ and $[a,2b-1)$. Introducing the vector of state variables in the frequency domain

$$\boldsymbol{z}^{\mathrm{T}}_{\mathscr{F}}(\omega,T) = \left[\boldsymbol{d}^{\mathrm{T}}_{\mathscr{F}}(\omega,T),\ (\mathrm{i}\omega)^{1/b}\boldsymbol{d}^{\mathrm{T}}_{\mathscr{F}}(\omega,T),\ \dots\ (i\omega)^{(2b-1)/b}\boldsymbol{d}^{\mathrm{T}}_{\mathscr{F}}(\omega,T)\right], \tag{29}$$

and appending to Eq. (28) the $2b-1$ identities

$$\sum_{j=1}^{2b-k} \boldsymbol{C}_{j+k}(\mathrm{i}\omega)^{1/b}(\mathrm{i}\omega)^{(j-1)/b}\boldsymbol{d}_{\mathscr{F}}^{\mathrm{T}}(\omega,T) = \sum_{j=1}^{2b-k} \boldsymbol{C}_{j+k}(\mathrm{i}\omega)^{j/b}\boldsymbol{d}_{\mathscr{F}}^{\mathrm{T}}(\omega,T), \quad k=1,2,\ldots,2b-1, \tag{30}$$

then a set of $2n\times 2b$ coupled algebraic equations is readily cast in the form

$$\left(\boldsymbol{A}\sqrt[b]{\mathrm{i}\omega}+\boldsymbol{B}\right)\boldsymbol{z}_{\mathscr{F}}(\omega,T) = \boldsymbol{g}_{\mathscr{F}}(\omega,T), \tag{31}$$

where $\boldsymbol{g}_{\mathscr{F}}^{\mathrm{T}}(\omega,T) = W_{\mathscr{F}}(\omega,T)\left[\boldsymbol{p}^{\mathrm{T}}\ \boldsymbol{0}\ \ldots\ \boldsymbol{0}\right]$, the involved matrices are symmetric and defined as

$$\boldsymbol{A} = \begin{bmatrix} \boldsymbol{C}_1 & \boldsymbol{C}_2 & \ldots & \boldsymbol{C}_{2b-1} & \boldsymbol{C}_{2b} \\ \boldsymbol{C}_2 & \boldsymbol{C}_3 & \ldots & \boldsymbol{C}_{2b} & \boldsymbol{0} \\ \vdots & \vdots & \ddots & \vdots & \vdots \\ \boldsymbol{C}_{2b-1} & \boldsymbol{C}_{2b} & \ldots & \boldsymbol{0} & \boldsymbol{0} \\ \boldsymbol{C}_{2b} & \boldsymbol{0} & \ldots & \boldsymbol{0} & \boldsymbol{0} \end{bmatrix} \quad \boldsymbol{B} = \begin{bmatrix} \boldsymbol{K} & \boldsymbol{0} & \ldots & \boldsymbol{0} & \boldsymbol{0} \\ \boldsymbol{0} & -\boldsymbol{C}_2 & \ldots & -\boldsymbol{C}_{2b-1} & -\boldsymbol{C}_{2b} \\ \vdots & \vdots & \ddots & \vdots & \vdots \\ \boldsymbol{0} & -\boldsymbol{C}_{2b-1} & \ldots & \boldsymbol{0} & \boldsymbol{0} \\ \boldsymbol{0} & -\boldsymbol{C}_{2b} & \ldots & \boldsymbol{0} & \boldsymbol{0} \end{bmatrix}. \tag{32}$$

Now, it is possible to diagonalize the involved matrix by placing the complex modal transformation $\boldsymbol{z}_{\mathscr{F}}(\omega,T) = \boldsymbol{\Psi}\boldsymbol{y}_{\mathscr{F}}(\omega,T)$ and premultiplying both terms by $\boldsymbol{\Psi}^{\mathrm{T}}$. That is,

$$\begin{aligned} \boldsymbol{\Psi}^{\mathrm{T}}\left(\boldsymbol{A}\sqrt[b]{\mathrm{i}\omega}+\boldsymbol{B}\right)\boldsymbol{\Psi}\,\boldsymbol{y}_{\mathscr{F}}(\omega,T) &= \boldsymbol{\Psi}^{\mathrm{T}}\boldsymbol{g}_{\mathscr{F}}(\omega,T) \\ \left(\boldsymbol{U}_{\mathbf{d}}\sqrt[b]{\mathrm{i}\omega}+\boldsymbol{V}_{\mathbf{d}}\right)\boldsymbol{y}_{\mathscr{F}}(\omega,T) &= \boldsymbol{\mu}_{\mathscr{F}}(\omega,T), \end{aligned} \tag{33}$$

where $\boldsymbol{\Psi}$ contains the eigenvectors of the matrix $\boldsymbol{D}=\boldsymbol{A}^{-1}\boldsymbol{B}$, the matrices $\boldsymbol{U}_{\mathbf{d}}=\boldsymbol{\Psi}^{\mathrm{T}}\boldsymbol{A}\boldsymbol{\Psi}$ and $\boldsymbol{V}_{\mathbf{d}}=\boldsymbol{\Psi}^{\mathrm{T}}\boldsymbol{B}\boldsymbol{\Psi}$ are diagonal (the subscript $\mathbf{d}$ stands for diagonal). Now, from Eq. (33) the response in the complex modal space is

$$\boldsymbol{y}_{\mathscr{F}}(\omega,T) = \left(\boldsymbol{U}_{\mathbf{d}}\sqrt[b]{\mathrm{i}\omega}+\boldsymbol{V}_{\mathbf{d}}\right)^{-1}\boldsymbol{\mu}_{\mathscr{F}}(\omega,T) = \boldsymbol{H}_{\mathbf{d}}(\omega)\boldsymbol{\mu}_{\mathscr{F}}(\omega,T), \tag{34}$$

where the transfer function matrix in the complex modal space $\boldsymbol{H}_{\mathbf{d}}(\omega) = (\boldsymbol{U}_{\mathbf{d}}\sqrt[b]{\mathrm{i}\omega}+\boldsymbol{V}_{\mathbf{d}})^{-1}$ is diagonal and each terms can be evaluated in closed from. In particular, the j-th diagonal term of such matrices is given as

$$H_j(\omega) = \frac{1}{u_j\sqrt[b]{\mathrm{i}\omega}+v_j} \tag{35}$$

being u_j and v_j the j-th terms of the diagonal matrices $\boldsymbol{U}_{\mathbf{d}}$ and $\boldsymbol{V}_{\mathbf{d}}$, respectively.

Defining all terms in Eq. (34), each term of the vector $\boldsymbol{y}_{\mathscr{F}}(\omega,T)$ can be readily obtained in analytical form and then the exact PSD matrix in the state variable domain can be derived. In particular,

$$\begin{aligned} \boldsymbol{S}_{\boldsymbol{z}}(\omega) &= \lim_{T\to\infty}\frac{\mathrm{E}\left[\boldsymbol{z}_{\mathscr{F}}^{*}(\omega,T)\boldsymbol{z}_{\mathscr{F}}^{\mathrm{T}}(\omega,T)\right]}{2\pi T} = \boldsymbol{\Psi}^{*}\lim_{T\to\infty}\frac{\mathrm{E}\left[\boldsymbol{y}_{\mathscr{F}}^{*}(\omega,T)\boldsymbol{y}_{\mathscr{F}}^{\mathrm{T}}(\omega,T)\right]}{2\pi T}\boldsymbol{\Psi}^{\mathrm{T}} \\ &= \boldsymbol{\Psi}^{*}\boldsymbol{H}_{\mathbf{d}}^{*}(\omega)\lim_{T\to\infty}\frac{\mathrm{E}\left[\boldsymbol{\mu}_{\mathscr{F}}^{*}\boldsymbol{\mu}_{\mathscr{F}}^{\mathrm{T}}(\omega)\right]}{2\pi T}\boldsymbol{H}_{\mathbf{d}}{}^{\mathrm{T}}(\omega)\boldsymbol{\Psi}^{\mathrm{T}} = \boldsymbol{\Psi}^{*}\boldsymbol{H}_{\mathbf{d}}^{*}(\omega)\boldsymbol{S}_{\boldsymbol{\mu}}(\omega)\boldsymbol{H}_{\mathbf{d}}{}^{\mathrm{T}}(\omega)\boldsymbol{\Psi}^{\mathrm{T}} \\ &= \boldsymbol{\Psi}^{*}\boldsymbol{H}_{\mathbf{d}}^{*}(\omega)\boldsymbol{\Psi}^{*\mathrm{T}}\boldsymbol{S}_{\boldsymbol{g}}(\omega)\boldsymbol{\Psi}\boldsymbol{H}_{\mathbf{d}}{}^{\mathrm{T}}(\omega)\boldsymbol{\Psi}^{\mathrm{T}}. \end{aligned} \tag{36}$$

this matrices has dimension $4nb\times 4bn$ and its first block of $2n\times 2n$ terms contains the matrix $\boldsymbol{S}_{\boldsymbol{d}}(\omega)$ of the Eq. (25). Each term of the matrices $\boldsymbol{S}_{\boldsymbol{z}}(\omega)$ can be evaluated in closed form. In particular, considering the i-th row and the r-th column of such matrices, the corresponding term is

$$S_{z,ir}(\omega) = \sum_{j}^{4bn}\sum_{l}^{4bn}\sum_{k}^{2n}\sum_{s}^{2n}\frac{\Psi_{il}^{*}\Psi_{sl}^{*}p_sS_{g,sk}(\omega)p_k\Psi_{kj}\Psi_{rj}}{\left(u_l^{*}\sqrt[b]{-\mathrm{i}\omega}+v_l^{*}\right)\left(u_j\sqrt[b]{\mathrm{i}\omega}+v_j\right)} = S_0\sum_{j}^{4bn}\sum_{l}^{4bn}\sum_{k}^{2n}\sum_{s}^{2n}\frac{\Psi_{il}^{*}\Psi_{sl}^{*}p_sp_k\Psi_{kj}\Psi_{rj}}{\left(u_l^{*}\sqrt[b]{-\mathrm{i}\omega}+v_l^{*}\right)\left(u_j\sqrt[b]{\mathrm{i}\omega}+v_j\right)} \tag{37}$$

where p_k denotes the k-th term of the influence vector $\boldsymbol{p}$, and Ψ_{kj} is the term of the k-th row and the j-th column of the eigenvector matrices $\boldsymbol{\Psi}$. The Eq. (37) is obtained by simple algebraic passages from Eq. (36) and it is valid for generic stochastic forcing processes once the matrix $\boldsymbol{S}_g(\omega)$ is known; for the case at hand $S_{g,sk}(\omega) = S_0$. The knowledge of the exact expression of the PSD and CPSD of the response by the Eq. (37) permits to apply the method in [52] to find the variance and the covariance of the response processes. In particular, denoting as $\sigma^2_{z,ir}$ the covariance between the i-th response process and the r-th one, the following relation hold true

$$\sigma^2_{z,ir} = 2\sum_{j}^{4bn}\sum_{l}^{4bn}\sum_{k}^{2n}\sum_{s}^{2n}\Re\left\{\Psi^*_{il}\Psi^*_{sl}p_s p_k \Psi_{kj}\Psi_{rj}R_{lj}\right\}, \tag{38}$$

where $\Re\{\cdot\}$ denotes the real part of the term inside the brackets, and R_{lj} is related to the residue of complex spectral moments of the response processes [52] and defined as

$$R_{lj} = \frac{S_0 \mathrm{i}(-1)^{-b}}{\sqrt{-1}v^*_l u_j - v_j u^*_l}\left\{\left(\frac{v^*_l}{u^*_l}\right)^{b-1}\left[b\log\left(\frac{u^*_l}{v^*_l}\sqrt[b]{i}\right)-\gamma\right] + \sqrt[b]{-1}\left(\frac{v_j}{u_j}\right)^{b-1}\left[b\log\left(\frac{u_j}{v_j}\sqrt[b]{i}\right)-\gamma\right]\right\}, \tag{39}$$

where γ is the Euler-Mascheroni constant. Obviously, when $i = r$ in Eq. (38) the expression becomes the variance of the i-th response process.

Eq.s (37) and (38) represent the analytical expression of the PSD/CPSD and variance/covariance of the response processes at steady state obtained with the aid of the fractional state variable analysis and with the complex modal transformation in frequency domain. The state variable approach introduced above can be used also in the time domain to perform Monte Carlo simulations to evaluate the stationary and non-stationary responses and their related statistics. Such approach does not provide analytical expressions but it is introduced in the next subsection for sake of completeness since it represents a valuable numerical tool to verify the accuracy of the presented analytical expressions.

3.2. Time-domain analysis

The state variable analysis and the complex modal transformation used in the previous subsection can be also applied to decouple the set of fractional differential equations in time domain [49] and it can be applied to any system ruled by coupled fractional differential equations. In particular, by using the state variable representation in Eq. (31) in time domain and by placing the modal transformation $\boldsymbol{z}(t) = \boldsymbol{\Psi}\boldsymbol{y}(t)$, the Eq. (33) leads to a set of decoupled fractional differential equations and each equation is of the kind

$$u_j\left(D^{1/b}_{0^+}y_j\right)(t) + v_j y_j(t) = \mu_j(t), \quad j = 1,2,3,\ldots,4bn, \tag{40}$$

that represents the equation of the motion of a fractional Kelvin-Voigt model with complex coefficients [48]. The impulse response function of the Eq. (40) is given as

$$h_j(t) = \frac{\sqrt[b]{t}}{t\,v_j}\sum_{k=0}^{\infty}\frac{\left(-v_j/u_j\sqrt[b]{t}\right)^k}{\Gamma(k/b+1/b)}, \tag{41}$$

and the modal response of the system in Eq. (40) can be evaluated by the Duhamel superposition integral. That is,

$$y_j(t) = \int_0^t h_j(t-\bar{t})\mu_j(\bar{t})d\bar{t}, \tag{42}$$

that has to be evaluated for $j = 1,2,3,\ldots,4bn$. In this way all terms of the vector $\boldsymbol{y}(t)$ are know and by the modal transformation also the vector of the state variable $\boldsymbol{z}(t)$ can be found. In particular, each term of such vector is

$$z_l(t) = \sum_{j=1}^{4bn}\sum_{k=1}^{2n}\Psi_{lj}\Psi_{jk}\int_0^t h_j(t-\bar{t})\mu_j(\bar{t})d\bar{t}, \quad l = 1,2,\ldots 4bn. \tag{43}$$

Obviously, the first $2n$ terms of the state variable vector represent the displacements $V_j(t)$ and the rotations $\Phi_j(t)$ of the system in Eq. (20). Eq. (43) can be used for the Monte Carlo simulations in order to determine the stationary and non-stationary response processes. This method is used in the numerical applications to evaluate the non-stationary variance and to verify the accuracy of the analytical equations presented in the previous subsection.

4. Numerical applications

Next, the proposed solution method is used to calculate the stochastic response of a cantilever non-local fractional beam forced by a Gaussian white noise with $S_0 = 1$. The purpose is to validate the proposed closed-form expressions (37) and (38) for the PSD and for the variance, as well as to show accuracy and efficiency of the proposed set of decoupled fractional equations (40), obtained from the fractional-order state-variable expansion, when performing time-domain Monte Carlo simulations. To this aim, the following results are provided for the deflection response along the beam:

(i) Eq. (37) for the PSD is compared with the corresponding PSD obtained from the set of coupled fractional equations (14), that is Eq. (24). Notice that Eq. (24) for the PSD requires numerical computation of the inverse matrix, with significant computational costs as the number of FEs increases.

(ii) Eq. (38) for the variance is compared with the corresponding one obtained from the area under the PSD (24).

(iii) The set of decoupled fractional equations (40) is numerically integrated to build 1000 samples of the response, the variance of which is finally compared with the proposed closed-form expression (38). Numerical integration of the decoupled fractional equations (40) is performed based on the analytical impulse response functions (41). The

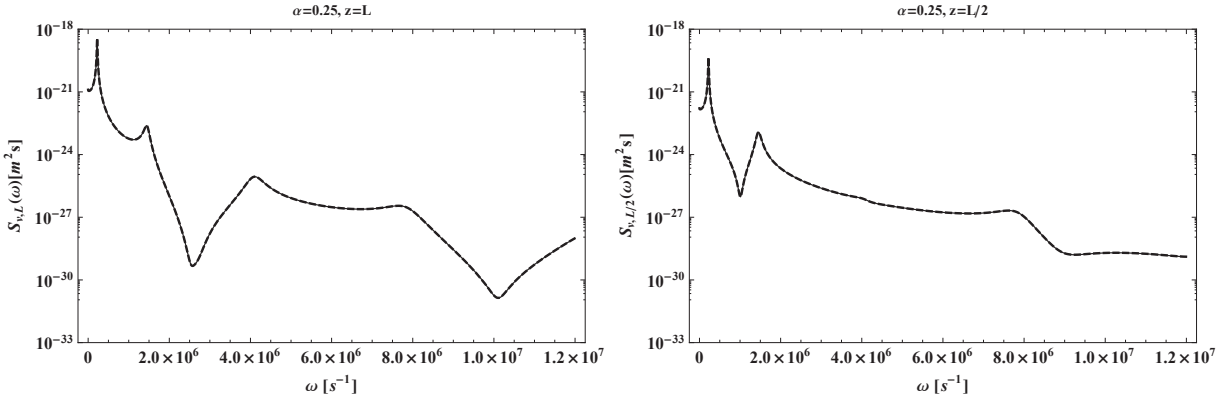

(a) (b)

Figure 3: PSD for the free-end and midpoint deflection with $\alpha = 0.25$: proposed closed-form expression (37) (thick dashed line); numerical solution from Eq. (24) (thin solid line).

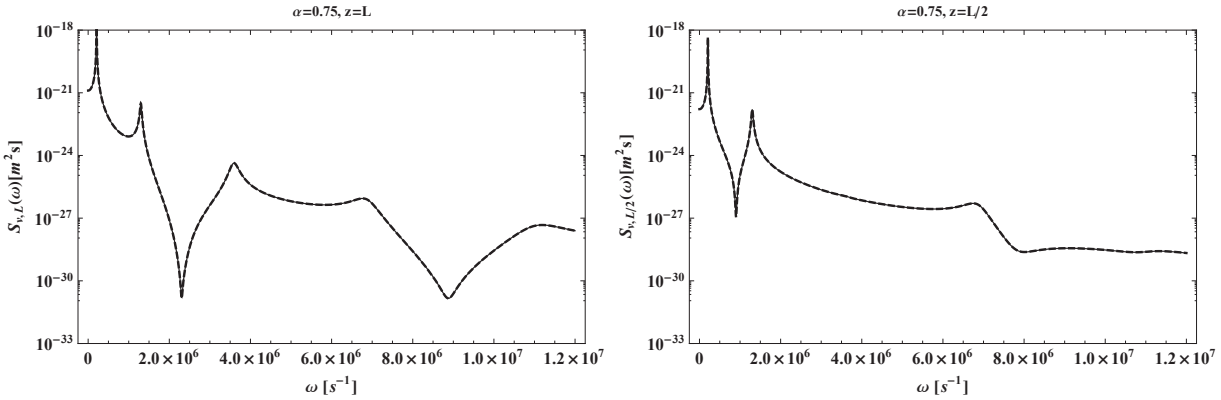

(a) (b)

Figure 4: PSD for the free-end and midpoint deflection with $\alpha = 0.75$: proposed closed-form expression (37) (thick dashed line); numerical solution from Eq. (24) (thin solid line).

$\alpha =$	0.25		0.75	
$z =$	L	$L/2$	L	$L/2$
σ_v^2 Eq. (38)	2.19×10^{-15}	2.68×10^{-16}	2.05×10^{-14}	2.43×10^{-15}
σ_v^2 Eq. (24)	2.22×10^{-15}	2.75×10^{-16}	2.07×10^{-14}	2.46×10^{-15}

Table 1: Comparison between the variances of the free-end and midpoint deflection evaluated with the proposed closed-form expression (38) and numerical integration of the PSD obtained with Eq. (24).

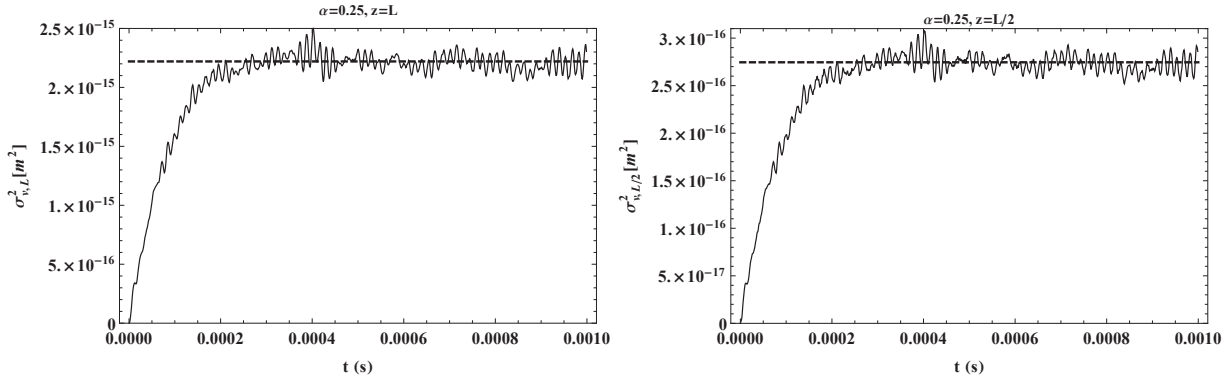

(a) (b)

Figure 5: Variance for the free-end and midpoint deflection, with $\alpha = 0.25$: evolutionary variance obtained by Monte Carlo simulation (1000 samples) from Eq. (43) (thin solid line); stationary variance obtained from the proposed closed-form expression (38) (thick dashed line).

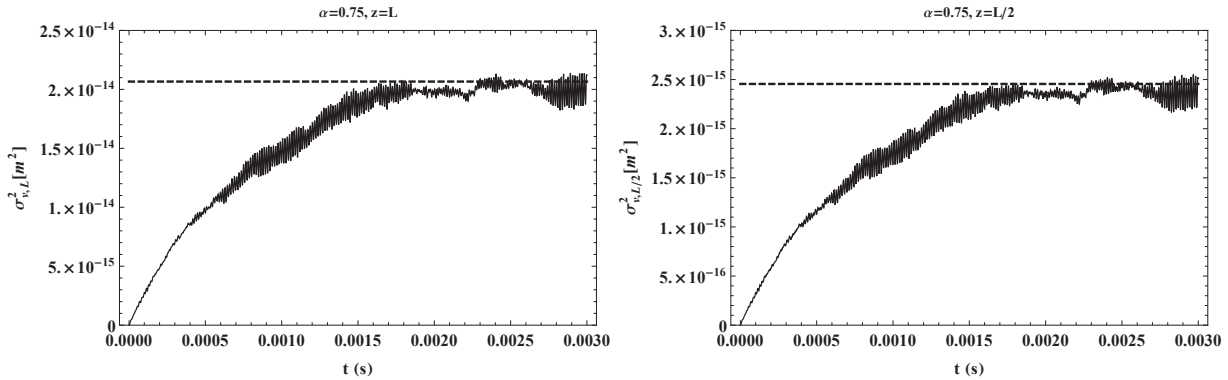

(a) (b)

Figure 6: Variance for the free-end and midpoint deflection, with $\alpha = 0.75$: evolutionary variance obtained by Monte Carlo simulation (1000 samples) from Eq. (43) (thin solid line); stationary variance obtained from the proposed closed-form expression (38) (thick dashed line).

case study is an epoxy microbeam with the following properties: length $L = 300\,\mu m$, rectangular cross section with dimensions $\mathrm{b} = 30\,\mu m$ (width) and $\mathrm{h} = 15\,\mu m$ (thickness), $E = 1.4\,GPa$, $\rho = 1000\,kg/m^3$; the selected attenuation functions are exponential:

$$g(x,\zeta) = \frac{C}{\mathrm{h}^2} \mathrm{e}^{\frac{|x-\zeta|}{\lambda}} \tag{44a}$$

$$\tilde{g}(x,\zeta) = \frac{\tilde{C}}{\mathrm{h}^2} \mathrm{e}^{\frac{|x-\zeta|}{\lambda}} \tag{44b}$$

Two different values of the fractional order are considered for the long-range interactions, namely $\alpha = 0.25$ and $\alpha = 0.75$; in both case the rational order that permits to obtain the vector state variable in Eq. (29) is $1/b = 1/4 = 0.25$.

The non local parameters in Eqs. (44) are: $\lambda = 20\ \mu m$, $\tilde{\lambda} = 20\ \mu m$, $C = 10^{11}\ Nm^{-6}$ and $\tilde{C} = 10^{10}\ Nm^{-6}$ for $\alpha = 0.25$ and $\tilde{C} = 10^{6}\ Nm^{-6}$ for $\alpha = 0.75$.
Figure 3 through Figure 6 show that the proposed closed-form expression (37) and (38) for PSD and variance are in excellent agreement with corresponding numerical one obtained from Eq. (24) for the considered points along the beam axis and values of fractional order α. As for the variances, a further comparison is made in Tab. 1 that shows very good agreement between the values evaluated by means of Eq.(38) and the numerical integration of the PSD evaluated with Eq. (24). Likewise, it is noticed that the proposed closed-form expression (38) for the variance matches very well the stationary value attained by the evolutionary variance, as computed from the proposed set of decoupled fractional equations (40). The same conclusions may be drawn also for other values of the fractional order alpha, but results are not included for brevity. Besides accuracy, the proposed solution method is easy to implement and computationally efficient. The method relies indeed on analytical expressions for non-local matrices $\boldsymbol{K}^{(nl)}$ and $\boldsymbol{C}^{(nl)}$ (see ref. [45] of the authors), closed-form expressions (37) for PSD and CPSD, closed-form expressions (38) for variance and covariance while time-domain numerical integration of the proposed set of decoupled fractional equations (40) can readily be performed using the analytical impulse response functions (41). Computational advantages are significant with respect to the classical numerical expression (24) for the PSD and CPSD or the classical computationally-expensive time-domain numerical integration of the set of coupled fractional equations (14), which requires specific tools of fractional calculus to discretize the time-dependent fractional derivatives [48]. In this respect, it is important to remark that the proposed solution method can readily be used also by engineers who are not necessarily familiar with specific tools of fractional calculus, which are not required to implement Eq. (37), (38) and Eq. (41).

5. Conclusions

In this paper the dynamic behaviour of non-local Timoshenko beam forced by a Gaussian white noise has been investigated. Long range interactions are modelled as both elastic and viscoelastic, the latter involving fractional derivative in the constitutive equation. Since the beam is discretized with the FE method, the mechanical behaviour of the system is ruled by a set of coupled fractional differential equations. Due to the non-local terms in the involved coefficient matrices the set of coupled fractional differential equations can not be decoupled with the standard method of modal analysis. For this reason, the dynamic response of the beam is studied by means of a fractional-order state-variable expansion and a complex modal transformation. In frequency domain this method allows to obtain closed form expressions of PSD/CPSD and variance/covariance of any response process along the beam axis. In time domain this approach permits to perform efficiently Monte Carlo simulations. In this way, stationary and non stationary response processes can be found and used to evaluate numerical statistics. The proposed method is easy to implement and does not require specific knowledge of fractional calculus, moreover numerical applications have shown the accuracy of results in comparison with more computational expensive numerical solutions. In particular, the numerical integrations of approximated PSD/CPSD and the Monte Carlo simulations have shown the precision of the analytical expressions obtained in frequency domain. Despite the fact that the application considered in this paper is a beam, the method is readily applicable to any kind of mechanical system with a finite number of degrees of freedom.

References

[1] Lu P, Lee HP, Lu C, Zhan PQ. Application of non local beam models for carbon nanotubes. Int J Solids Struct 2007; 44(16): 5289-5300
[2] Reddy JN. Non-local theories for bending, buckling and vibration of beams. Int J Eng Sci 2007; 45(2-8): 288-307
[3] Aydogdu M. A general non-local beam theory: Its application to nanobeam bending, buckling and vibration. Physica E 2009; 41(9): 1651-1655.
[4] Park SK, Gao XL. Bernoulli-Euler beam model based on a modified couple stress theory. J Micromech Microeng 2006; 16(11): 2355-2359
[5] Kong S, Zhou S, Nie Z, Wang K. The size-dependent natural frequency of Bernoulli-Euler micro-beams. Int J Eng Sci 2008; 46(5): 427-437.
[6] Challamel N, Wang CM. The small length scale effect for a non-local cantilever beam: A paradox solved. Nanotechnology 2008; 19(34): 345703
[7] Zhang YY, Wang CM, Challamel N. Bending, buckling,and vibration of micro/nanobeams by hybrid nonlocal beam model. J Eng Mech 2010; 10.1061/(ASCE)EM.1943-7889.0000107, 562-574.
[8] Ma HM, Gao X-L, Reddy JN. A microstructure dependent Timoshenko beam model based on a modified couple stress theory. J Mech Phys Solids 2008; 56(12): 3379-3391.

[9] Tarasov VE, Aifantis EC. Non-standard extensions of gradient elasticity: Fractional non-locality, memory and fractality.Commun Nonlinear Sci Numer Simulat 2015; 22(1-3): 197-227.
[10] Pradhan SC. Nonlocal finite element analysis and small scale effects of CNTs with Timoshenko beam theory. Finite Elem Anal Des 2012; 50: 8-20.
[11] Yang Y, Lim CW. Non-classical stiffness strengthening size effects for free vibration of a non local nanostructure. Int J Mech Sci 2012; 54(1): 57-68.
[12] Lam DCC, Yang F, Chong ACM, Wang J, Tong P. Experiments and theory in strain gradient elasticity. J Mech Phys Solids 2003; 51(8): 1477-1508.
[13] McFarland AW, Colton JS (2005). Role of material microstructure in plate stiffness with relevance to microcantilever sensors. J Micromech Microeng 2005; 15(5): 1060-1067.
[14] Apuzzo A, Barretta R, Luciano R, Marotti de Sciarra F, Penna R. Free vibrations of Bernoulli-Euler nano-beams by the stress-driven nonlocal integral model. Compos Part B 2017; 123: 105-11.
[15] Apuzzo A, Barretta R, Canadija M, Feo L, Luciano R, Marotti de Sciarra F. A closed-form model for torsion of nanobeams with an enhanced nonlocal formulation. Compos Part B 2017; 108: 315-24.
[16] Barretta R, Feo L, Luciano R, Marotti de Sciarra F. Application of an enhanced version of the Eringen differential model to nanotechnology. Compos Part B 2016; 96: 274-80.
[17] Lakes RS. Experimental micro mechanics methods for conventional and negative Poissons ratio cellular solids as Cosserat continua. J Eng Mater Technol 1991; 113(1): 148-155.
[18] Aifantis EC. Gradient effects at macro, micro, and nano scales. J Mech Behav Mater 1994; 5(3): 355-375.
[19] Barretta R, Feo L, Luciano R, Marotti de Sciarra F, Penna R. Functionally graded Timoshenko nanobeams: A novel nonlocal gradient formulation. Compos Part B 2016; 100: 208-19.
[20] Barretta R, Feo L, Luciano R, Marotti de Sciarra F. An Eringen-like model for Timoshenko nanobeams. Compos Struct 2016; 139: 104-10.
[21] Qian D, Wagner GJ, Liu WK, Yu M-F, Ruoff RS. Mechanics of carbon nanotubes. Appl Mech Rev 2002; 55(6): 495-533.
[22] Mancusi G, Fabbrocino F, Feo L, Fraternali F. Size effect and dynamic properties of 2D lattice materials. Compos Part B 2017; 112: 235-42.
[23] Arash B, Wang Q. A review on the application of nonlocal elastic models in modeling of carbon nanotubes and graphenes. Comput Mater Sci 2012; 51(1): 303-313.
[24] Tang PY. Interpretation of bend strength increase of graphite by the couple stress theory. Comput Struct 1983; 16(1-4): 45-49.
[25] Poole WJ, Ashby MF, Fleck NA. Micro-hardness of annealed and work-hardened copper polycrystals. Scr Mater 1996; 34(4): 559-564.
[26] Wang LF, Hu HY. Flexural wave propagation in single-walled carbon nanotube. Phys Rev B 2005; 71(19): 195412-195418.
[27] Romano G, Barretta R. Stress-driven versus strain-driven nonlocal integral model for elastic nano-beams. Compos Part B 2017; 114: 184-88.
[28] Lei Y, Friswell MI, Adhikari S. A Galerkin method for distributed systems with non-local damping. Int J Solids Struct 2006; 43(11-12): 3381-3400.
[29] Friswell MI, Adhikari S, Lei Y. Non-local finite element analysis of damped beams. Int J Solids Struct 2007; 44(22-23): 7564-7576.
[30] Russell DL (1992). On mathematical models for the elastic beam with frequency-proportional damping. Control and estimation in distributed parameter systems, H. T. Banks, ed., SIAM, Philadelphia, 125-169.
[31] Banks HT, Inman DJ. On damping mechanism in beams. J Appl Mech 1991; 58(3): 716-723.
[32] Lopez SG, Fernandez JS. Vibrations in Euler-Bernoulli beams treated with non-local damping patches. Comput Struct 2012; 108: 125-134.
[33] Banks HT, Wang Y, Inman DJ. Bending and shear damping in beams: Frequency domain estimation techniques. J Vib Acoust 1994; 116(2): 188-197.
[34] Lei Y, Murmu T, Adhikari S, Friswell MI. Dynamic characteristics of damped viscoelastic nonlocal Euler-Bernoulli beams. Eur J Mech A/Solids 2013; 42: 125-136.
[35] Barretta, R., Feo, L., and Luciano, R. Torsion of functionally graded nonlocal viscoelastic circular nanobeams. Compos Part B 2015; 72: 217-222.
[36] Karlicic, D., Cajic, M., Murmu, T., Adhikari, S. (2015). Nonlocal longitudinal vibration of viscoelastic coupled double-nanorod systems. Eur J Mech A/Solids, 49, 183-196.
[37] Ghorbanpour-Arani AH, Rastgoo A, Sharafi MM, Kolahchi R, GhorbanpourArani A. Nonlocal viscoelasticity based vibration of double viscoelastic piezoelectric nanobeam systems. Meccanica 2016; 51: 25-40.
[38] Payton D, Picco L, Miles MJ, Homer ME, Champney AR. Modelling oscillatory flexure modes of an atomic force microscope cantilever in contact mode whilst imaging at high speed. Nanotechnology 2012; 23(26): 265702.
[39] Murmu T, Adhikari S. (2012). Nonlocal frequency analysis of nanoscale biosensors. Sensor Actuat A-Phys 2012; 173(1): 41-48.
[40] Chen C, Ma M, Liu J, Zheng Q, Xu Z. Viscous damping of nanobeam resonators: Humidity, thermal noise, and a paddling effect. J Appl Phys 2011; 110(3): 034320.
[41] Lee J, Lin C. The magnetic viscous damping effect on the natural frequency of a beam plate subject to an in-plane magnetic field. J Appl Mech 2010; 77(1): 011014.
[42] Su Y, Wei H, Gao R, Yang Z, Zhang J, Zhong Z, Zhang Y. Exceptional negative thermal expansion and viscoelastic properties of graphene oxide paper. Carbon 2012; 50: 2804-2809.
[43] Di Paola M, Failla G, Zingales M. Physically-based approach to the mechanics of strong non-local linear elasticity theory. J Elast 2009; 97(2): 103-130.
[44] Di Paola M, Failla G, Zingales M. The mechanically-based approach to 3D non-local linear elasticity theory: Long-range central interactions. Int J Solids Struct 2010a; 47(18-19): 2347-2358.
[45] Alotta G, Failla G, Zingales M. Finite element method for a nonlocal Timoshenko beam model. Finite Elem Anal Des 2014; 89: 77-92.
[46] Di Paola M, Failla G, Zingales M. Non-local stiffness and damping models for shear-deformable beams. Eur J Mech A/Solids 2013; 40: 69-83.
[47] Alotta G, Failla G, Zingales M. Finite-element formulation of a nonlocal hereditary fractional-order Timoshenko beam. J Eng Mech 2017; 143(5): D4015001.

[48] Podlubny I. (1999). Fractional differential equations: An introduction to fractional derivatives, fractional differential equations, some methods of their solution and some of their applications, Academic Press, New York.
[49] Alotta G, Failla G, Pinnola FP. Stochastic analysis of a non-local fractional viscoelastic bar forced by Gaussian white noise. ASCE-ASME J Risk and Uncert in Eng Sys, Part B: Mech Eng 2017; 3(3): 030904.
[50] Fuchs MB. Unimodal beam elements. Int J Solids Struct 1991; 27(5): 533–545.
[51] Autori G, Cluni F, Gusella V, Pucci P. Effects of the Fractional Laplacian Order on the Nonlocal Elastic Rod Response. ASCE-ASME J Risk and Uncert in Eng Sys, Part B: Mech Eng 2017; 3(3): 030902
[52] Pinnola FP. Statistical correlation of fractional oscillator response by complex spectral moments and state variable expansion. Commun Nonlinear Science Num Simulat 2016; 39: 343-359.